Supplemental information

Supplemental Figures

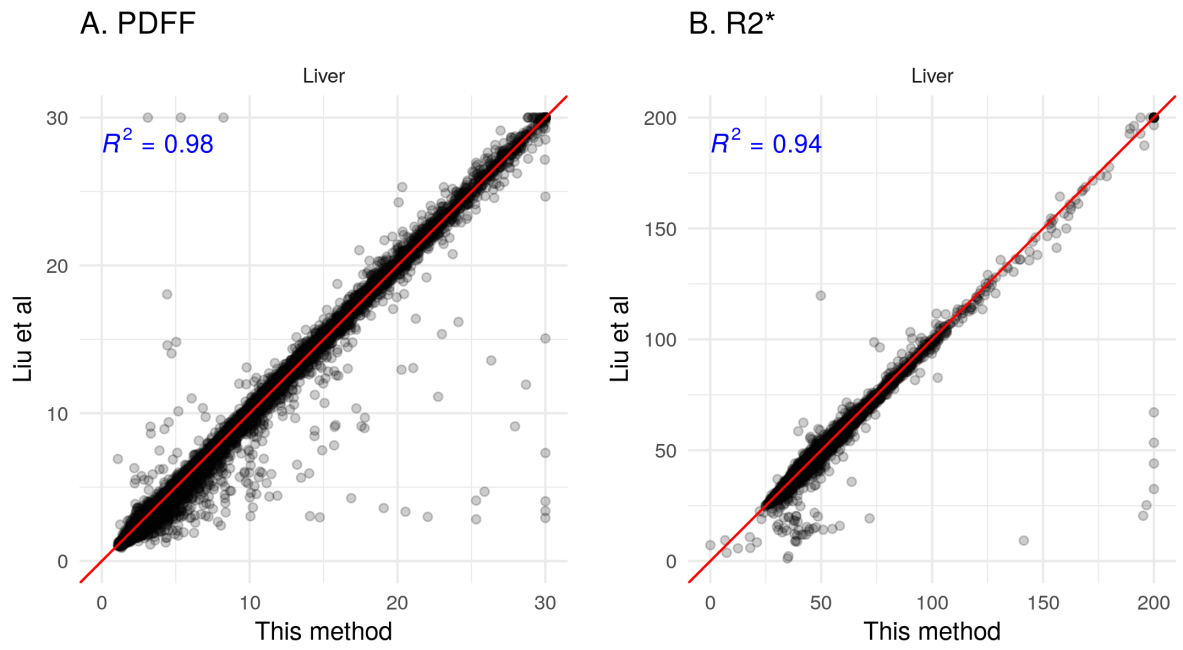

Figure S1: Scatter plot comparing direct neural network-based segmentation[1] in a dedicated 2D slice (y-axis) with opportunistic resampling[2] from the 3D (Dixon) acquisition (x-axis) A) median liver PDFF (in %) and (B) median liver R2* (in s^{-1}) (n=38,400).

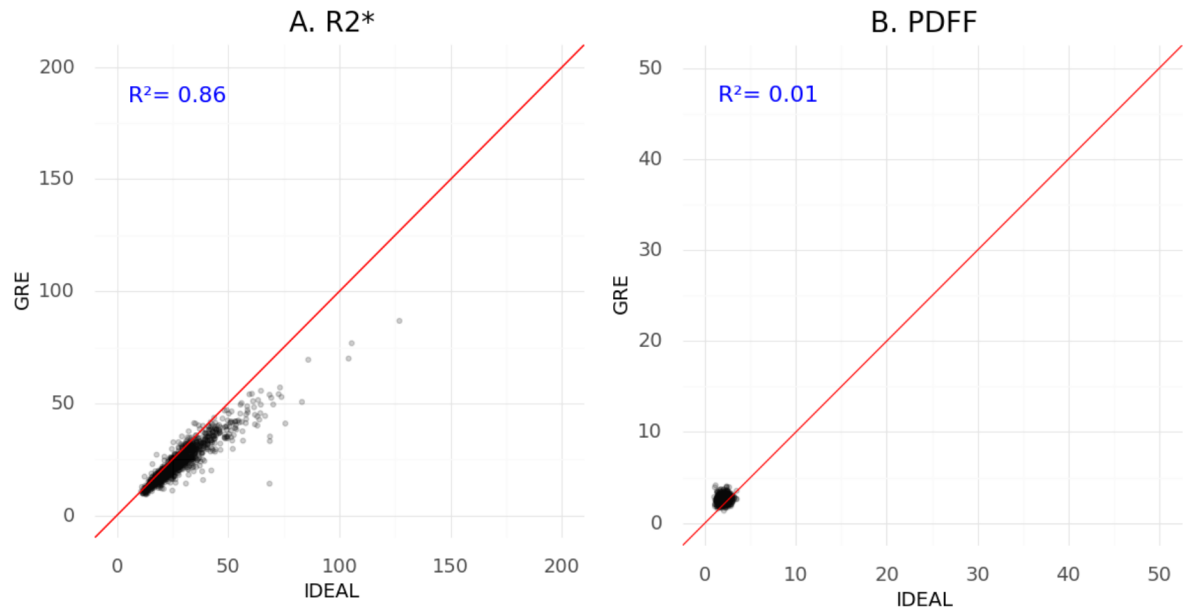

Figure S2. Relationship between parameters measured in the spleen in n=1,364 UKBB subjects with both GRE and IDEAL single-slice multi-echo acquisitions. Scatter plots for median R2* (A) measurements (in s^{-1}) and PDFF in % (B). Pearson's correlation between the measures is given in blue.

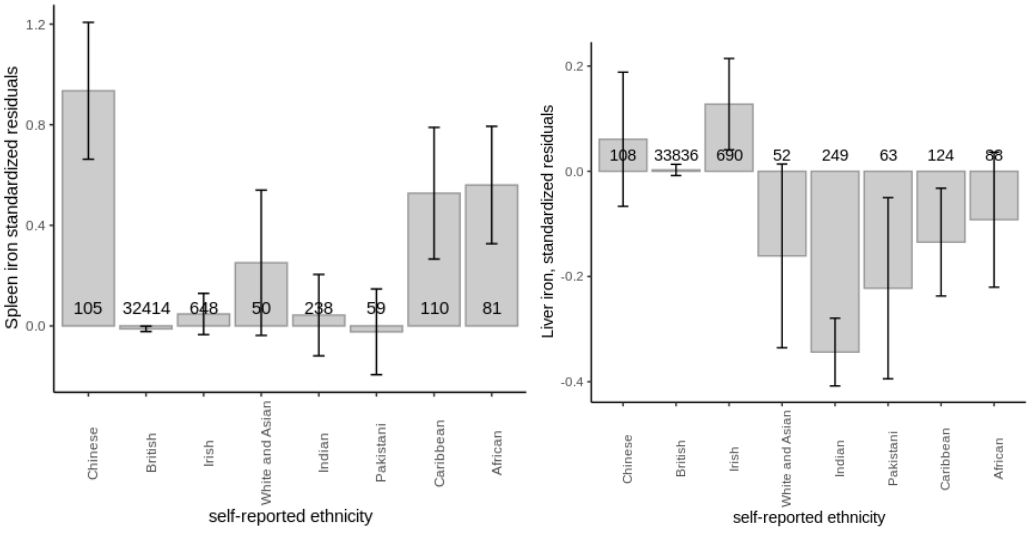

Figure S3: Spleen iron varies by self-reported ethnicity. (A) Spleen iron displayed as standardized residuals after adjustment for age, sex, study center, scan date and time. (B) Liver iron content displayed as standardized residuals after adjustment for the same covariates. Only groups with >50 individuals with imaging phenotypes are shown. 95% CIs are shown.

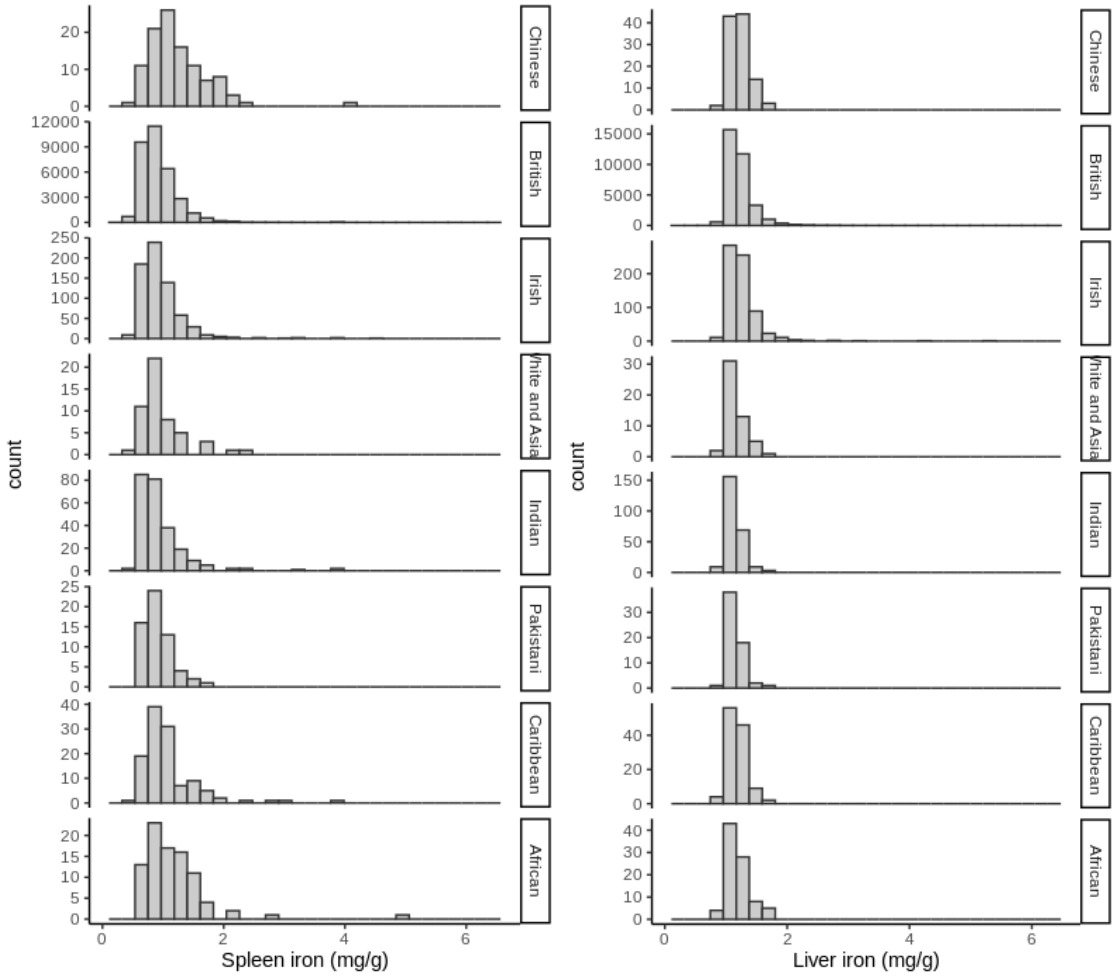

Figure S4: **Spleen iron (in mg/g) varies by self-reported ethnicity but with a limited sample size for non-European groups**. Left panel: Histogram of spleen iron in mg/g by self-report ethnicity. Right panel: Histogram of liver iron content in mg/g by self-report ethnicity.

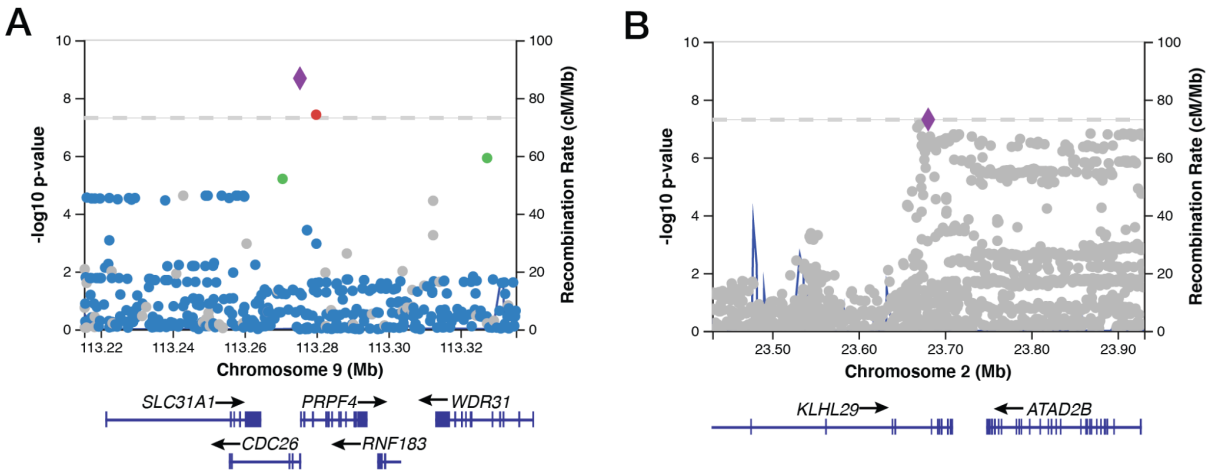

Figure S5: Lead SNPs associated with spleen iron in the *PRPF4/CDC26* and *KLHL29* loci after statistical fine-mapping. (A) The lead SNP in the *PRPF4/CDC26* locus on chromosome 9 is rs41276777[A]. (B) The lead SNP in the *KLHL29* locus on chromosome 2 is rs115697725[G].

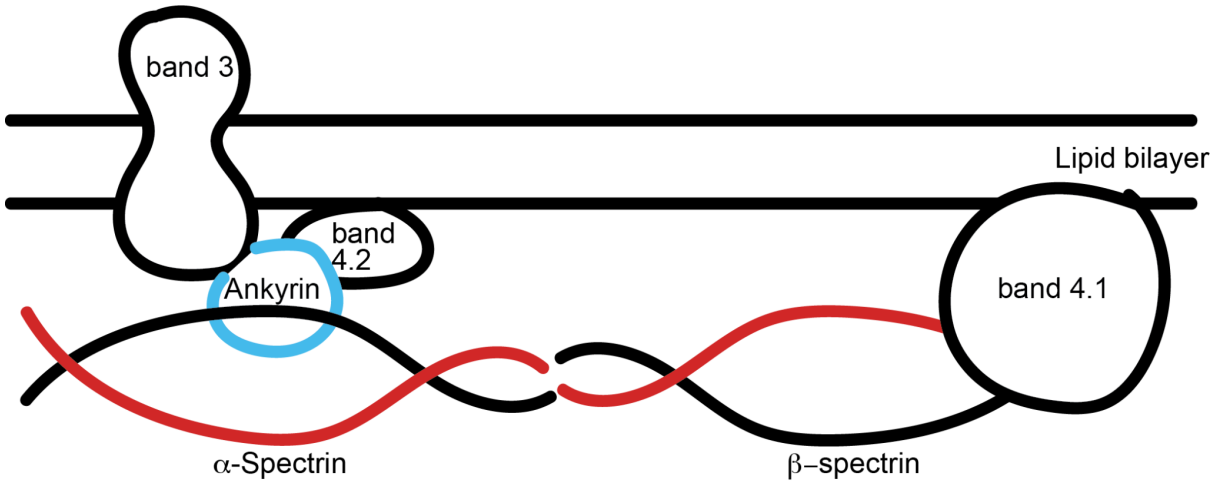

Figure S6: Simplified cartoon of a cross-section of an red blood cell membrane cytoskeleton. Cytoskeletal protein ankyrin (encoded by the *ANK1* gene) is shown in blue, and alpha-spectrin (encoded by *SPTA1*) is shown in red. Alpha and beta spectrins contain antin-binding domains and associate to form anti-parallel heterodimers which interact to form tetramers. Ankyrins anchor anion exchangers in the lipid bilayer to the spectrin filaments. The anion exchanger band 3, as well as cytoskeletal proteins band 4.1, and band 4.2, are depicted for reference. Adapted from Delaunay et al.[3]

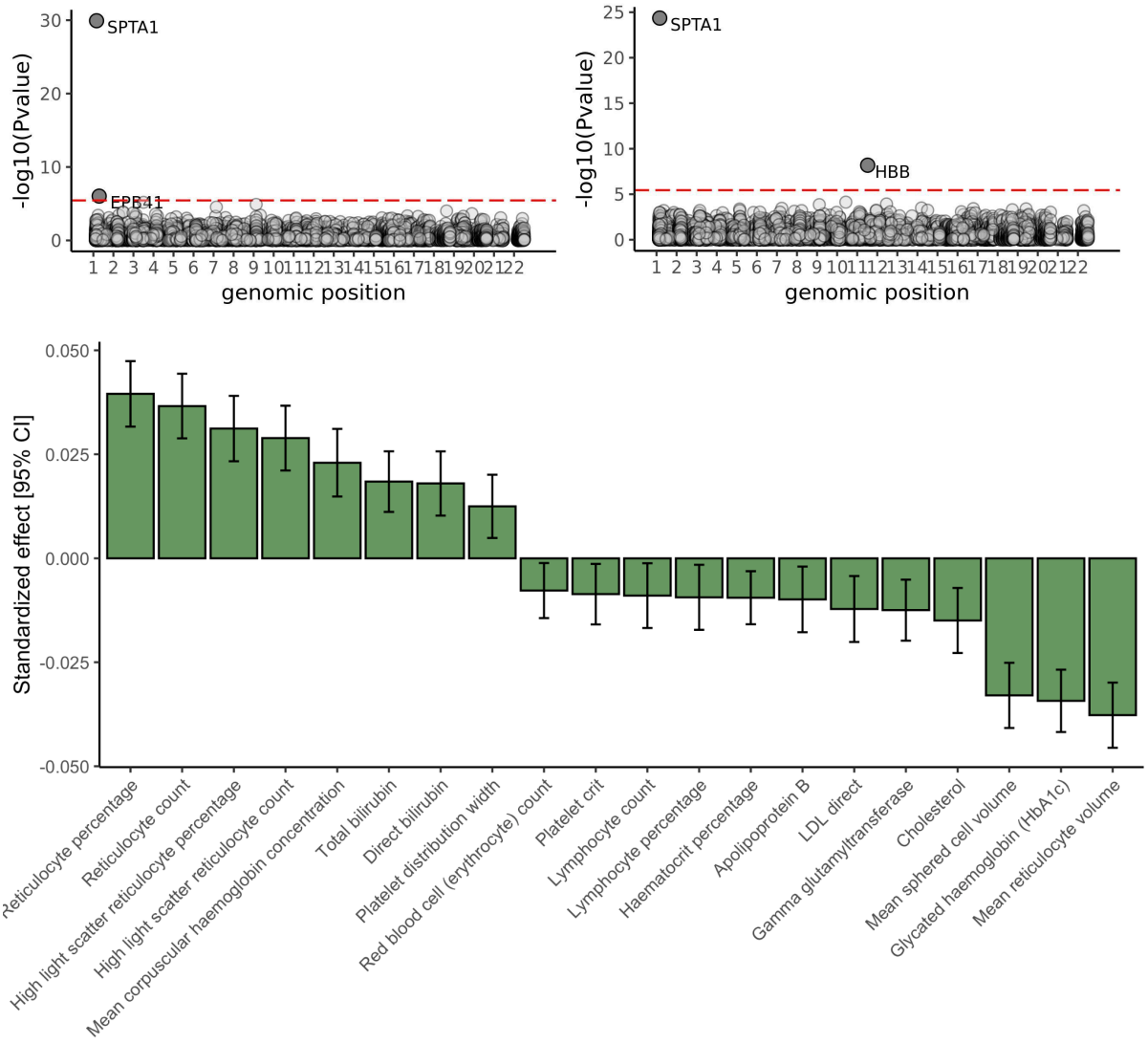

Figure S7: Predicted loss-of-function variation in *SPTA1* is associated with RBC biomarkers, platelet biomarkers, bilirubin, cholesterol, and glycated hemoglobin (HbA1c) in 167,243 exomes via rare variant association study (RVAS). Top left: Exome-wide association study (ExWAS) of reticulocyte percentage identifies two components of red blood cell membrane architecture: *SPTA1* (encoding alpha-spectrin) and *EPB41* (encoding band 4.1). **Top right:** ExWAS of mean reticulocyte volume identifies *SPTA1* and *HBB*, encoding beta hemoglobin Bonferroni significance is shown with the dashed red line. **Bottom:** ExWAS across a panel of 31 quantitative hematological traits for rare coding mutations in *SPTA1* recapitulated signatures of hereditary spherocytosis, including increased reticulocyte percentage, mean corpuscular hemoglobin concentration, bilirubin; and decreased mean sphered cell volume and mean reticulocyte volume.

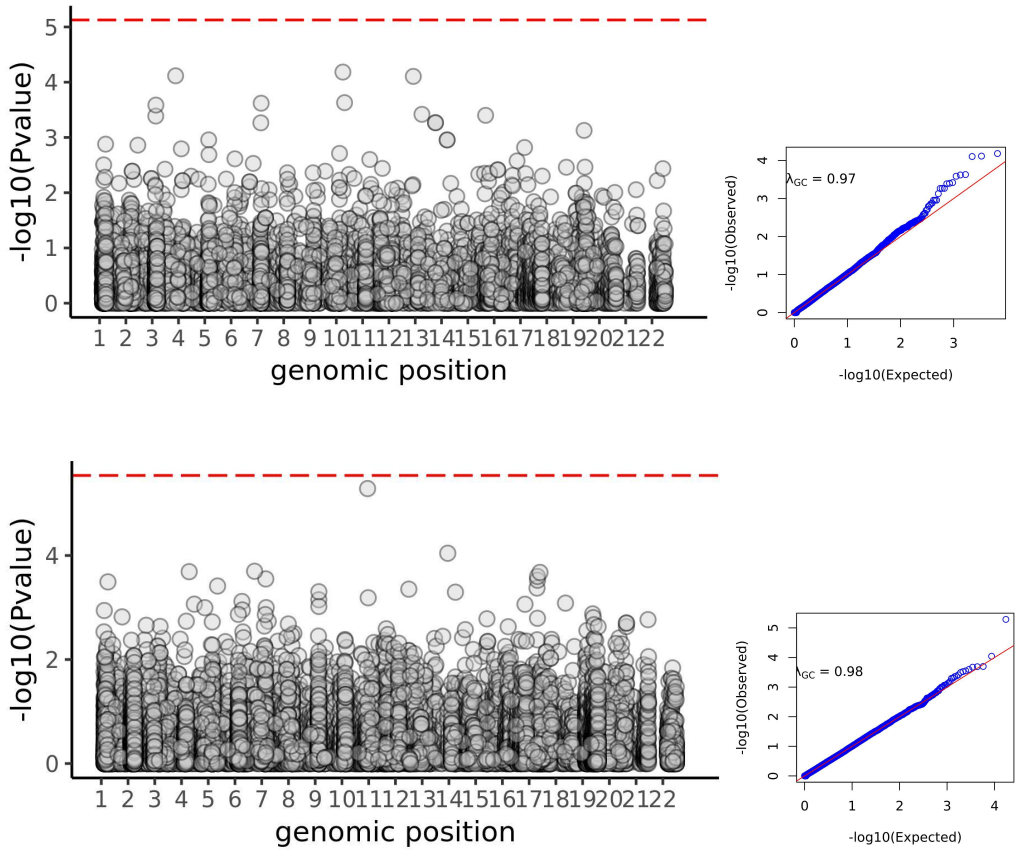

Figure S8: Rare variant burden testing to identify associations with spleen iron. **Top panel:** Rare variant burden testing of loss-of-function variation in 18,240 exomes. 286,546 variants in 6,686 genes (minor allele count >=5) were tested. QQ plot is shown at right. **Bottom panel:** Rare variant burden testing of predicted deleterious missense variation. 2,919,962 variants in 17,298 genes (minor allele count >=5) were tested. QQ plot is shown at right.

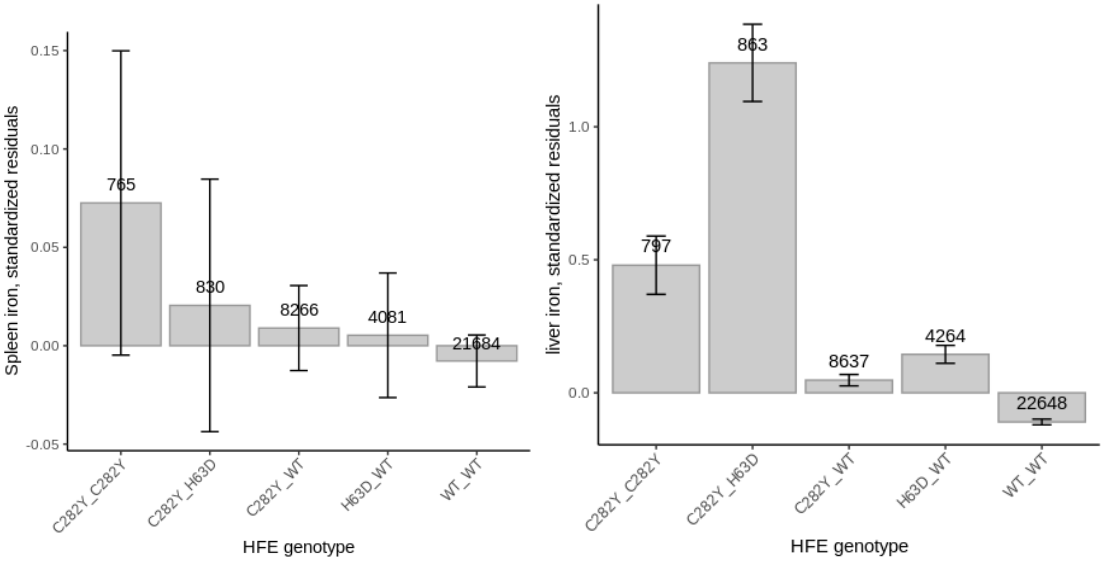

Figure S9: Spleen iron in HFE carriers, homozygotes, compound heterozygotes and non-carriers. (A) HFEp.Cys282Tyr homozygosity, HFEp.Cys282Tyr/p.His63Asp compound heterozygosity, and HFEp.Cys282Tyr carrier status are not associated with significant differences in spleen iron. Standardized residuals of liver iron content, following adjustment for age, genetic sex, study center, scan date and time (B) Carrier status at the HFE locus affects liver iron. Standardized residuals of spleen iron, following adjustment for age, genetic sex, study center, scan date and time.

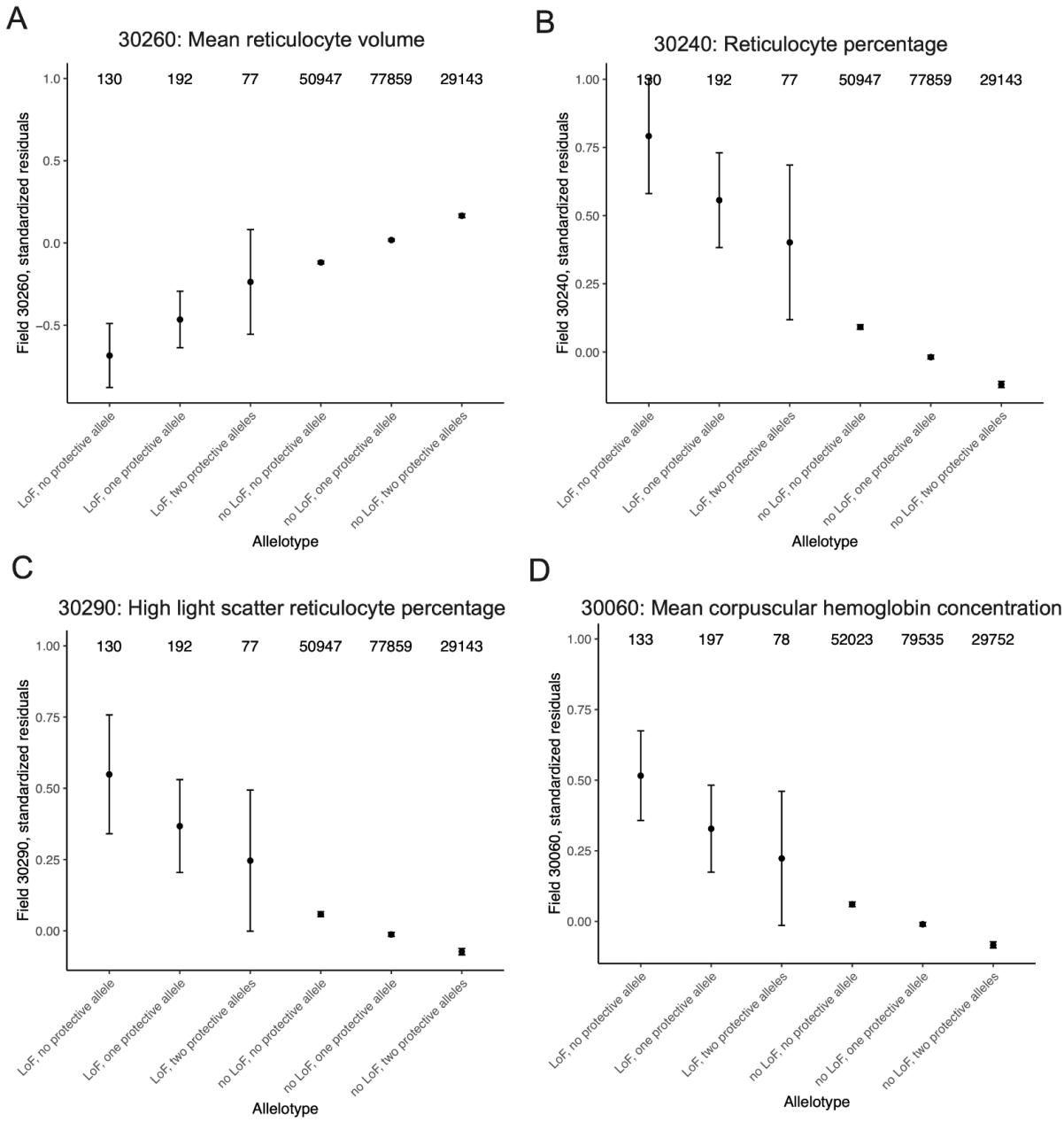

Figure S10: Allelotype analysis comparing individuals with and without the common, 'protective' alleles in *SPTA1* or *ANK1*, and with and without putative deleterious alleles in one of six hereditary spherocytosis (HS) genes. Standardized residuals, adjusted for age, sex, and global principal components of ancestry are shown for four red blood cell parameters: (A)

mean reticulocyte volume (B) reticulocyte percentage (C) high light scatter reticulocyte percentage, (D) mean corpuscular hemoglobin concentration. Sample sizes are shown at top. 95% confidence intervals around group means are shown.

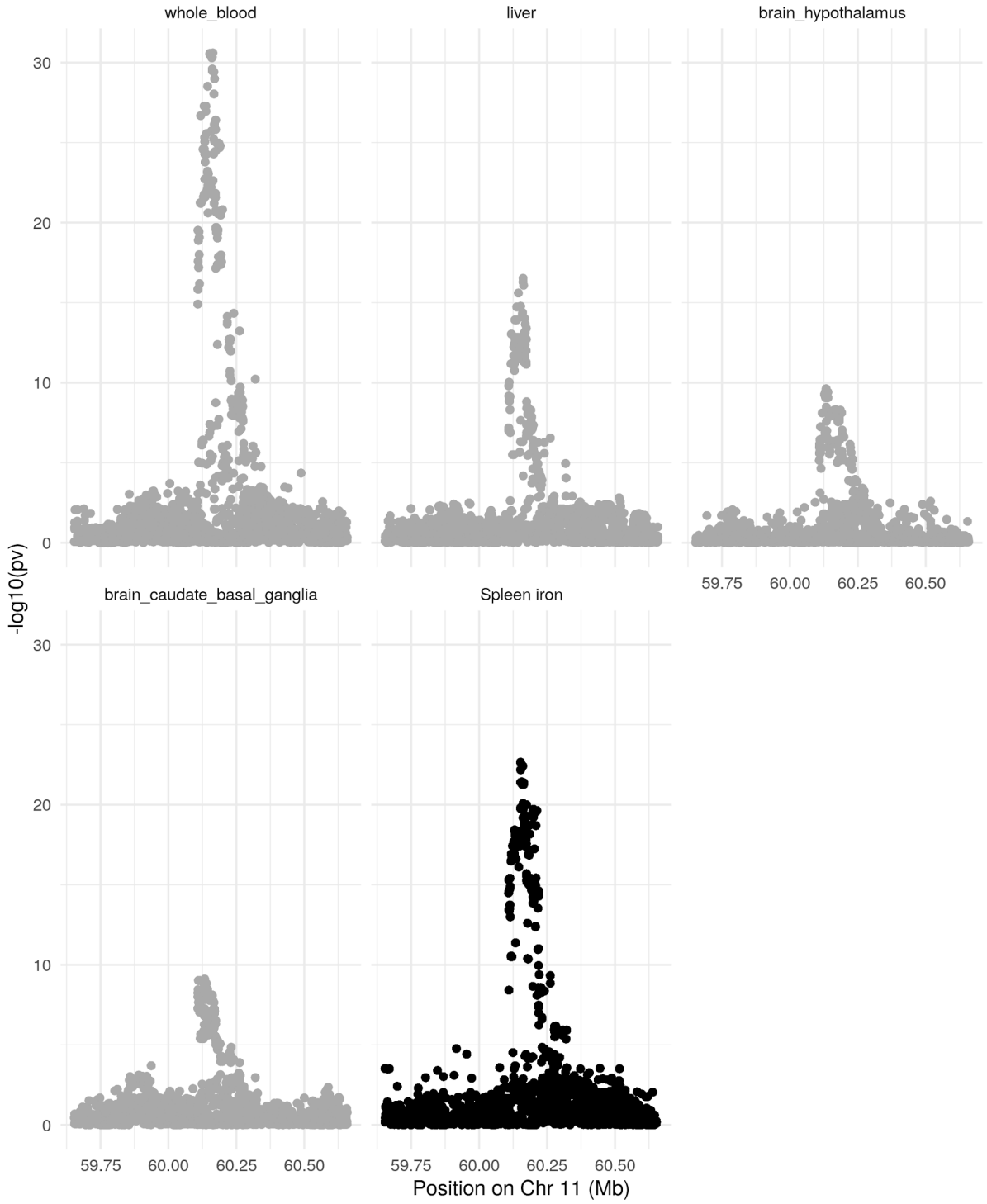

Figure S11: Colocalization of spleen iron and expression of *MS4A14* in various tissues. Tissues are ordered by the strength of the colocalization.

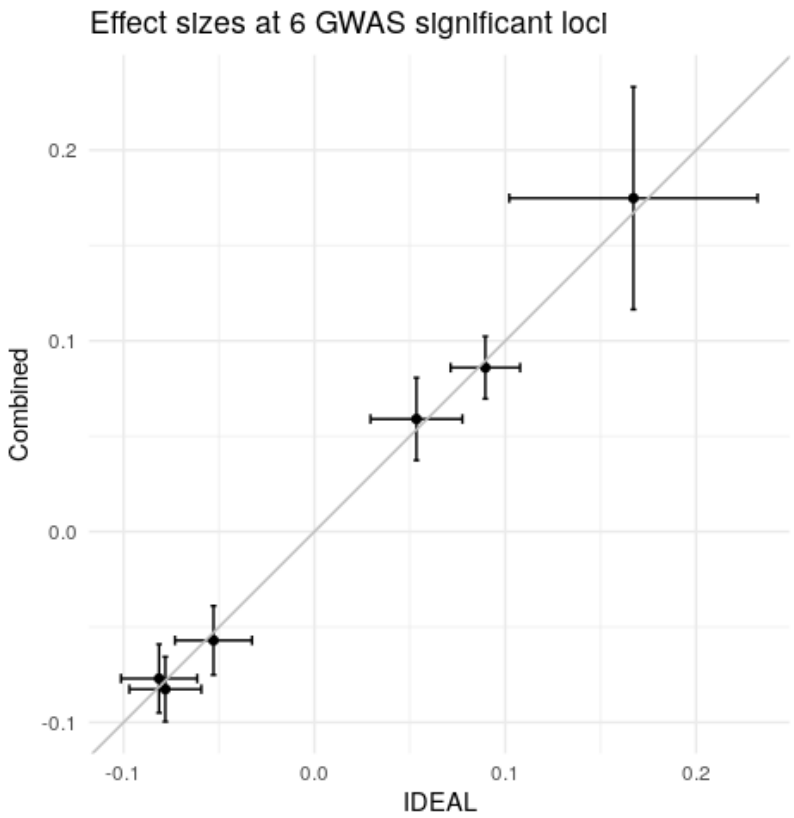

Figure S12: Effect size and error bars (2 * standard error) for 6 GWAS-significant loci from the IDEAL-only dataset (x-axis) and combined IDEAL and GRE dataset (y-axis).

Supplemental Tables

		IDEAL		GRE	
	Organ	n	mean(sd) [min-max]	n	mean(sd) [min-max]
Iron (mg/g)	**Liver**	29920	1.24 (0.302) [0.203 - 6.96]	9960	1.23 (0.287) [0.829 - 4.2]
	Spleen	28682	0.924 (0.349) [0.202 - 6.44]	9581	0.913 (0.422) [0.335 - 4.2]
PDFF (%)	**Liver**	29920	5.1 (4.93) [1.09 - 51]	9960	5.82 (6.65) [0 - 52.3]
	Spleen	28682	2.55 (0.392) [0 - 4.98]	9581	2 (0.442) [0 - 4.93]
R2*	**Liver**	29920	41 (11.9) [0.0311 - 266]	9960	40.1 (9.8) [24.7 - 126]
	Spleen	28682	28.4 (13.7) [0.00744 - 246]	9581	26.9 (11.6) [0 - 135]

Table S1: Values for spleen and liver iron, PDFF, and R2* divided into GRE and IDEAL acquisitions in the UK Biobank.

Percentile	Female	Male	Both
0.025	0.527	0.554	0.536
0.05	0.552	0.586	0.565
0.075	0.571	0.612	0.588
0.1	0.589	0.634	0.607
0.125	0.604	0.653	0.624
0.15	0.619	0.673	0.641
0.175	0.634	0.691	0.656
0.2	0.647	0.707	0.671
0.225	0.659	0.722	0.686
0.25	0.672	0.739	0.702
0.275	0.685	0.754	0.715
0.3	0.699	0.770	0.730
0.325	0.713	0.783	0.745
0.35	0.726	0.798	0.760
0.375	0.739	0.813	0.774
0.4	0.753	0.829	0.788
0.425	0.768	0.846	0.802
0.45	0.780	0.861	0.818
0.475	0.795	0.877	0.834
0.5	0.810	0.895	0.849
0.525	0.826	0.910	0.864
0.55	0.840	0.929	0.882
0.575	0.856	0.948	0.900

0.6	0.873	0.968	0.917
0.625	0.890	0.987	0.937
0.65	0.908	1.010	0.957
0.675	0.927	1.031	0.977
0.7	0.949	1.054	1.001
0.725	0.972	1.081	1.025
0.75	0.996	1.106	1.050
0.775	1.021	1.141	1.081
0.8	1.051	1.174	1.111
0.825	1.087	1.213	1.148
0.85	1.121	1.257	1.190
0.875	1.164	1.312	1.238
0.9	1.219	1.378	1.299
0.925	1.290	1.457	1.376
0.95	1.380	1.580	1.485
0.975	1.551	1.803	1.693

Table S2: Percentiles of the distribution of spleen iron concentration in the UK Biobank, stratified by males and females. Iron concentration is provided as mg/g.

		Female		**Male**	
	Organ	**n**	**mean(s.d.) [min-max]**	**n**	**mean(s.d.) [min-max]**
Iron (mg/g)	Liver	21,388	1.22 (0.29) [0.2-7.29]	22,877	1.25 (0.33) [0.2-6.99]
	Spleen	19,960	0.87 (0.29) [0.17-6.68]	21,804	0.96 (0.34) [0.17-6.48]

Table S3: Spleen iron mean concentration in the UK Biobank, stratified by males and females. Iron cncentration is provided as mg/g.

Table S4: Results from phenome-wide association study of spleen iron with 2,346 traits including medical history, lifestyle factors, self-reported questionnaires, and other abdominal MRI derived traits. Provided as an Excel spreadsheet.

Table S5: Results form phenome-wide association study of spleen iron with 857 disease diagnosis codes. Provided as an Excel spreadsheet.

Table S6: Genetic correlations between spleen iron and 288 traits in the UK Biobank. Provided as an Excel spreadsheet.

Trait 1	Trait 2	rg	se	z	p
Spleen iron	Serum ferritin (Bell et al, 2021)	0.5592	0.0973	5.7476	9.05E-09
Spleen iron	Serum iron (Bell et al, 2021)	0.211	0.1099	1.9209	5.47E-02
Spleen iron	TSAT (Bell et al, 2021)	0.2661	0.0875	3.0401	2.36E-03
Spleen iron	TIBC (Bell et al, 2021)	-0.2042	0.0867	-2.3546	1.85E-02
Spleen iron	Liver iron (Liu et al, 2020)	0.2479	0.1038	2.3888	1.69E-02
Spleen iron	Pancreas iron (Liu et al, 2020)	-0.0685	0.1615	-0.4243	6.71E-01
Spleen iron	Pancreas fat (Liu et al, 2020)	0.1027	0.1138	0.9027	3.67E-01
Spleen iron	Liver fat (Liu et al, 2020)	-0.0508	0.1125	-0.4517	6.51E-01
Spleen iron	Lung volume (Liu et al, 2020)	-0.0674	0.0974	-0.6925	4.89E-01
Spleen iron	Spleen volume (Liu et al, 2020)	-0.2357	0.0983	-2.3979	1.65E-02
Spleen iron	ASAT volume (Liu et al, 2020)	-0.0301	0.1066	-0.2823	7.78E-01
Spleen iron	VAT volume (Liu et al, 2020)	0.0669	0.104	0.6434	5.20E-01
Spleen iron	Kidney volume (Liu et al, 2020)	-0.1435	0.0938	-1.5301	1.26E-01
Spleen iron	Pancreas volume (Liu et al, 2020)	-0.0242	0.1049	-0.2306	8.18E-01
Spleen iron	Liver volume (Liu et al, 2020)	-0.2853	0.0935	-3.0522	2.27E-03

Table S7: Genetic correlations between spleen iron and six previously published blood and organ iron traits: ferritin, serum iron, transferrin saturation (TSAT), and total iron binding capacity (TIBC)[4], and pancreas and liver iron[1].

Index variant	Trait 1	Trait 2	N snps	PP0	PP1	PP2	PP3	PP4
1:158580069:C:T:b37	spleen iron	serum ferritin	4155	0.00E+00	0.00E+00	5.73E-17	1.00E+00	4.92E-18
8:41630447:G:A:b37	spleen iron	serum ferritin	3172	0.00E+00	0.00E+00	2.08E-11	1.00E+00	6.48E-13
1:158580069:C:T:b37	spleen iron	serum iron	4159	0.00E+00	0.00E+00	6.75E-17	1.00E+00	2.02E-18
8:41630447:G:A:b37	spleen iron	serum iron	3118	0.00E+00	0.00E+00	2.10E-11	1.00E+00	5.07E-13
1:158580069:C:T:b37	spleen iron	TSAT	4157	0.00E+00	0.00E+00	5.73E-17	1.00E+00	1.10E-18
8:41630447:G:A:b37	spleen iron	TSAT	3139	1.47E-11	7.08E-01	4.62E-12	2.22E-01	7.08E-02
1:158580069:C:T:b37	spleen iron	TIBC	4155	0.00E+00	0.00E+00	5.73E-17	1.00E+00	1.31E-18
8:41630447:G:A:b37	spleen iron	TIBC	3133	0.00E+00	0.00E+00	2.08E-11	1.00E+00	1.54E-12
1:158580069:C:T:b37	spleen iron	pancreas iron	4487	4.97E-17	9.15E-01	4.30E-18	7.93E-02	6.02E-03
8:41630447:G:A:b37	spleen iron	pancreas iron	3492	1.83E-11	8.78E-01	2.40E-12	1.15E-01	7.07E-03
1:158580069:C:T:b37	spleen iron	liver iron	4487	4.61E-17	8.49E-01	7.89E-18	1.45E-01	5.47E-03

8:41630447:G:A:b37	spleen iron	liver iron	3492	1.90E-11	9.14E-01	1.46E-12	7.01E-02	1.60E-02

Table S8: Colocalization test results for genome-wide significant loci from the spleen iron GWAS with loci from six previously published blood and organ iron traits. TIBC, total iron-binding capacity; TSAT, trasferrin saturation. PP0 through PP4, colocalization probabilities.

Table S9: Colocalization test results for genome-wide significant loci from the spleen iron GWAS with expression quantitative trait loci (eQTLs) from 56 tissues of the GTex consortium (version 8). Provided as an Excel spreadsheet.

Table S10: Colocalization test results from genome-wide significant loci from the spleen iron study with hematological assays. Provided as an Excel spreadsheet.

Trait	**BCX2 cohort**	**rs_id**	**locus**	**effect allele**	**other allele**	**beta**	**se**	**p**
MCHC	AA	rs2479868	*SPTA1*	T	C	-0.033	0.015	3.1E-02
MCHC	EA	rs2479868	*SPTA1*	T	C	-0.035	0.004	1.0E-17
MCHC	H/L	rs2479868	*SPTA1*	T	C	-0.072	0.026	5.7E-03
MCHC	AA	rs4737010	*ANK1*	A	G	-0.057	0.013	7.0E-06
MCHC	EA	rs4737010	*ANK1*	A	G	-0.032	0.004	6.0E-13
MCHC	H/L	rs4737010	*ANK1*	A	G	-0.110	0.027	5.3E-05
MRV	AA	rs2479868	*SPTA1*	T	C	0.015	0.015	3.0E-01
MRV	EA	rs2479868	*SPTA1*	T	C	0.028	0.004	1.1E-11
MRV	H/L	rs2479868	*SPTA1*	T	C	0.015	0.016	3.5E-01
MRV	AA	rs4737010	*ANK1*	A	G	0.029	0.012	1.9E-02
MRV	EA	rs4737010	*ANK1*	A	G	0.023	0.005	3.1E-07
MRV	H/L	rs4737010	*ANK1*	A	G	0.043	0.017	1.4E-02
Monocyte count	AA	rs950802	*MS4A7*	A	G	0.022	0.012	7.8E-02
Monocyte count	EA	rs950802	*MS4A7*	A	G	0.012	0.005	1.5E-02
Monocyte count	H/L	rs950802	*MS4A7*	A	G	0.001	0.017	9.3E-01

Table S11: Replication analysis of *SPTA1* and *ANK1* associations with erythrocyte parameters in an independent cohort of the Blood Cell Consortium, representing East Asian (EA), African-American (AA), and Hispanic/Latino (H/L) populations.

Study	**N**	**Cohort**	**Age (years) mean±SD (range)**	**Form in which Iron overload originally presented Mean (range) units**	**Calculated Spleen iron (mg/g) mean (range)**
Schwenzer et al., 2008	129	Healthy volunteers	47.9 ± 11.4 (2-70)	T2* = 43.9 (14.4-113.6) ms	0.78 (0.43-1.97)

Anderson et al., 2001	15	Healthy volunteers	31 ± 3.7 (26-39)	T2* = 56±22 ms (ns)	0.66 (not provided)
Aslan et al., 2021	25	Sickle cell disease	**46.3 ± 13.6	R2* = 127.9 (80.4–182.3) s-1	3.45 (2.24-4.83)
Aslan et al., 2021	15	Hereditary hemochromatosis		R2* = 25.8 (18.9–35.2) s-1	0.86 (0.68-1.10)
Aslan et al., 2021	17	**β**-Thalassemia		R2* = 58.2 (45.5–72.3) s-1	1.68 (1.36-2.04)
Kolnagou et al 2012	16	**β**-Thalassemia	29.6 ± 4.4 (25-37)	T2* = 22.6 (1-73) ms	6.09 (0.55-25.60)
Çetinçakmak et al., 2020	92	**β**-Thalassemia	12.8 (4-34)	T2* = 9.24 (0.75-48.75) ms	2.95 (0.72-34.07)
França et al., 2018	56	Mixed liver disease	44.7 ± 13.8 (19-77)	R2* = 40 (IQR 18-51) s-1	1.22 (0.66-1.50)

Table S12. Comparative data from spleen iron measured by MRI in healthy volunteers and patient groups. T2* published values were converted into R2* values using the equation R2* = 1000/T2*. R2* published values were converted into [FE} in mg/g[5]. *Mean age only provided for mixed cohort, ↟Mean values calculated from individual patient values provided in the publication. MRI measurement of spleen iron may be expressed as signal intensity ratio based on T2w or T2*w imaging, T2, R2, T2* or R2*[6] or converted into values in mg/g using formulas derived from liver studies[5,7]. Older methods using changes in T2 relaxation are not as sensitive for mild or moderate spleen iron overload.[8] The upper range of T2* measures are higher than those measured using R2*, limiting direct comparison[9], furthermore, the relationship between R2 and R2* is different in the liver and spleen therefore R2 measurements may underestimate spleen iron[10], as such, they have not been included in this comparison.

Supplemental methods

Image Acquisition

We used the UK Biobank (UKBB) liver single-slice multi-echo MRI and the neck-to-knee Dixon MRI[11] in 44,265 subjects. For the first approximately 10,000 subjects, a gradient-echo (GRE) sequence was used, and subsequently an IDEAL[12] sequence was used (1,364 participants had both and contained the spleen). The liver slice covers the abdominal width generally including the spleen due to its position relative to the liver. **Figure 1** shows a coronal view of the neck-to-knee Dixon and the location of the liver 2D slice in red **(A)**, the estimated iron content for the liver and spleen in the multi-echo slice **(B)**.

GRE and IDEAL acquisitions

For quantitative MRI, we estimated the proton density fat fraction (PDFF) and R2* from the single-slice liver multi-echo data.[13] The R2* values were converted into iron concentrations.[5,14] Using the 1,364 participants with both the IDEAL and GRE acquisitions, we compared the R2* and PDFF measurements (**Figure S2**). Spleen PDFF in the GRE and IDEAL acquisitions were not correlated, supporting the idea that measurements of spleen PDFF via MRI are the result of noise reconstruction.[15] We therefore did not perform subsequent analysis on the PDFF measurements but included them for completeness as a negative result. Spleen R2* in the GRE and IDEAL acquisitions were strongly correlated (R^2=0.86).

To combine data from the GRE and IDEAL acquisitions, we first ranked the measurements within each modality. Where individuals had both measurements, we averaged the ranks. We then applied an inverse normal transformation and performed subsequent analyses using these residuals.

In order to report population-level iron concentration values while accounting for systematic differences between the acquisitions, for individuals with only GRE R2* measures, we applied a linear transformation. This transformation was derived by fitting a linear model to the 1,364 individuals with spleen R2* measurements for both IDEAL and GRE modalities:

$$R2^*_{IDEAL} = -1.276 + 1.2366 * R2^*_{GRE}$$

We then transformed R2* to iron (mg/g) as previously described.[5,14]

Validation of opportunistic resampling strategy

In order to validate our opportunistic resampling strategy used to obtain 2D spleen masks, we used direct neural network-based liver 2D segmentations from a previous study[1] and compared those to opportunistic resampling of the liver (**Figure S1).** For n=38,400, the results of opportunistic resampling against dedicated 2D liver segmentation shows a correlation of 0.98 for proton density fat fraction (PDFF) and 0.94 for R2*.

MRI-derived PDFF in the spleen is noise

While measurement of spleen fat was possible, with measured values ranging between 0 and 4.98% (**Table S1**), close scrutiny of these measurements for n=1,364 subjects who had two different acquisitions covering the same anatomy indicate a level of background noise (**Figure S2B**; R^2=0.01) leading us to agree with Hong et al.[15], that MRI measured spleen fat is at the level of background noise and cannot be meaningfully quantified. By contrast, spleen iron was reproducibly measured from both GRE and IDEAL (**Figure S2A**; R^2=0.86). Therefore, we focused subsequent analyses on spleen iron. Spleen iron is shown in **Table 1** as mean ± standard deviation.

Identification of GRE acquisitions with high iron content

Through the quality control process, it has come to our attention that the GRE echo times in the UKBB abdominal MRI protocol are not short enough to quantify iron when it is exceeding a threshold (approximately 4 mg/g). High iron concentrations have a superparamagnetic effect that distorts the local magnetic field resulting in a faster decay of transverse magnetization.[16] Values beyond this threshold are not detected in GRE and would be falsely assigned a low value unless flagged up. However, this issue may be accurately identified from the magnitude data across echo times. Using the 2D organ segmentations, we calculated the average signal intensity for each echo time. When the decay of these values had a drastic signal dropoff and the average values of the longest echo time magnitude images displayed no decay, we estimated that the iron is mischaracterized. We assigned a maximum iron value of 4.2 mg/g to 66 (0.67% of n= 9615 GRE participants; 0.15% of n=44711 total participants). To verify that including these participants with a censored value did not substantially affect overall results, we compared effect sizes with and without the GRE participants at the six genome-wide significant loci and found that effect sizes were highly correlated (R2>0.99), suggesting minimal impact due to the outlying GRE acquisitions (Figure S12).

Filtering self-reported ancestry for outliers

Self-reported ethnicity continental ancestry (European, South Asian, African, and East Asian) was obtained from the UKBB (field 21000) and principal component analysis performed using common (minor allele frequency >=0.05), independent (r^2<0.2), autosomal markers, in Hardy Weinberg equilibrium (p>1e-10), excluding regions of long-range linkage disequilibrium. FlashPCA v2.1 was used to calculate the first 10 principal components (PCs). Centroid distance was calculated by subtracting the population PC mean from the individual's PC, squaring, and dividing by the variance for that PC. Ancestry outliers were identified as extreme values on a histogram of centroid distance for PCs 1-3.

Identification of clinical carriers of *HFE,* hemoglobin, and *G6PD* alleles

A version of ClinVar was downloaded on February 1, 2021, from https://ftp.ncbi.nlm.nih.gov/pub/clinvar/vcf_GRCh37/. Pathogenic, likely pathogenic, and pathogenic/likely pathogenic variants were selected with a level of evidence of either a single submission with criteria provided, multiple submitters agree, or reviewed by an expert panel (there are no variants in hemoglobin genes with a practice guideline). Genotypes were calculated using PLINK v1.90 and R 3.6.3 to assess compound genotypes.

Supplemental results

Spleen iron varies by ethnicity

Spleen iron varied by self-reported ethnicity, even after pruning ancestry outliers and adjusting for age, sex, study center, scan date, and time ($p_{Kruskal\text{-}Wallis}$=2.1e-20; Methods, **Figure S4**). Even after removal of the British group (n=32,414) which was considerably larger than the other groups, there were differences in group means ($p_{Kruskal\text{-}Wallis}$=1.1e-17). We performed a similar analysis using liver iron, adjusted for the same covariates, and observed differences in group means ($p_{Kruskal\text{-}Wallis}$=2.1e-4; **Figure S4**). We note that the non-European groups were of

small sample size in this study, and larger sample sizes are needed to confirm these observations.

HFE carriers and compound heterozygotes have elevated spleen iron as compared with non-carriers

Hereditary hemochromatosis (HH) is a recessive Mendelian disorder characterized by accumulation of iron in the liver, blood and other tissues and is most commonly caused by missense variants in the *HFE* gene, which regulates iron uptake into hepatocytes in the liver. We examined two missense variants, HFEp.Cys282Tyr and HFEp.His63Asp, both of which segregate in the UKBB at high frequency (HFEp.Cys282Tyr: minor allele frequency (MAF) = 0.146 [95% CI 0.145 - 0.146] HFEp.His63Asp: MAF = 0.073 [95% CI 0.073 - .074]). While we observed elevated liver iron in C282Y and H63D carriers, compound heterozygotes, and homozygotes (**Figure S9A**), we did not observe any effects of HH carrier status on spleen iron, after adjustment for covariates (**Figure S9B**).

Thalassemia is a blood disorder characterized by low levels of hemoglobin. Although there was only one participant with a confirmed diagnosis in the imaging cohort, we identified putative carriers of mutations in globin genes characterized as pathogenic or likely pathogenic in ClinVar. We detected 345 mutations in globin genes (*HBA, HBB, HBC, HBD, HBE, HBF, HBH,* and *HBS*) asserted as pathogenic or likely pathogenic in ClinVar. Of those, only three variants in HBA and 20 variants in *HBB* segregated within the entire UKBB. All of these segregating variants were extremely rare, with the most common variant being rs33946267[C] in HBB, with a minor allele frequency of(MAF) of =3.2e-4 in the entire UKBB. None of these carriers overlapped with the imaging cohort, precluding further analysis of thalassemia carriers.

Glucose-6-phosphate dehydrogenase (G6PD) deficiency is a genetic metabolic abnormality particularly in males, caused by deficiency of the enzyme encoded by *G6PD* which is associated with RBC dysfunction. We identified 15 pathogenic variants underlying G6PD deficiency. Here, three variants did segregate in the imaging subcohort, most commonly rs1050828[C], with a minor allele frequency of 1.2e-3. Within the imaging cohort, there were 19 males with one of three *G6PD* pathogenic mutations. We compared spleen iron in *G6PD* carriers to non-carriers in males, but did not observe a significant difference at this sample size (**Figure S5**).

Supplemental References

1. Liu, Y., Basty, N., Whitcher, B., Bell, J.D., Sorokin, E.P., van Bruggen, N., Louise Thomas, E., and Cule, M. (2021). Genetic architecture of 11 organ traits derived from abdominal MRI using deep learning. eLife *10*,.

2. Basty, N., Liu, Y., Cule, M., Louise Thomas, E., Bell, J.D., and Whitcher, B. (2020). Automated Measurement of Pancreatic Fat and Iron Concentration Using Multi-Echo and

T1-Weighted MRI Data. 2020 IEEE 17th International Symposium on Biomedical Imaging (ISBI).

3. Delaunay, J. (2002). Molecular basis of red cell membrane disorders. Acta Haematol. *108*, 210–218.

4. Bell, S., Rigas, A.S., Magnusson, M.K., Ferkingstad, E., Allara, E., Bjornsdottir, G., Ramond, A., Sørensen, E., Halldorsson, G.H., Paul, D.S., et al. (2021). A genome-wide meta-analysis yields 46 new loci associating with biomarkers of iron homeostasis. Commun Biol *4*, 156.

5. Wood, J.C., Enriquez, C., Ghugre, N., Tyzka, J.M., Carson, S., Nelson, M.D., and Coates, T.D. (2005). MRI R2 and R2* mapping accurately estimates hepatic iron concentration in transfusion-dependent thalassemia and sickle cell disease patients. Blood *106*, 1460–1465.

6. Sirlin, C.B., and Reeder, S.B. (2010). Magnetic resonance imaging quantification of liver iron. Magn. Reson. Imaging Clin. N. Am. *18*, 359–381, ix.

7. St Pierre, T.G., Clark, P.R., Chua-anusorn, W., Fleming, A.J., Jeffrey, G.P., Olynyk, J.K., Pootrakul, P., Robins, E., and Lindeman, R. (2005). Noninvasive measurement and imaging of liver iron concentrations using proton magnetic resonance. Blood *105*, 855–861.

8. Arrivé, L., Thurnher, S., Hricak, H., and Price, D.C. (1990). Magnetic resonance imaging of splenic iron overload. Eur. J. Radiol. *10*, 98–104.

9. Fernandes, J.L. (2018). MRI for Iron Overload in Thalassemia. Hematol. Oncol. Clin. North Am. *32*, 277–295.

10. Brewer, C.J., Coates, T.D., and Wood, J.C. (2009). Spleen R2 and R2* in iron-overloaded patients with sickle cell disease and thalassemia major. J. Magn. Reson. Imaging *29*, 357–364.

11. Littlejohns, T.J., Holliday, J., Gibson, L.M., Garratt, S., Oesingmann, N., Alfaro-Almagro, F., Bell, J.D., Boultwood, C., Collins, R., Conroy, M.C., et al. (2020). The UK Biobank imaging enhancement of 100,000 participants: rationale, data collection, management and future directions. Nat. Commun. *11*, 2624.

12. Reeder, S.B., Pineda, A.R., Wen, Z., Shimakawa, A., Yu, H., Brittain, J.H., Gold, G.E., Beaulieu, C.H., and Pelc, N.J. (2005). Iterative decomposition of water and fat with echo asymmetry and least-squares estimation (IDEAL): Application with fast spin-echo imaging. Magnetic Resonance in Medicine *54*, 636–644.

13. Bydder, M., Ghodrati, V., Gao, Y., Robson, M.D., Yang, Y., and Hu, P. (2020). Constraints in estimating the proton density fat fraction. Magn. Reson. Imaging *66*, 1–8.

14. McKay, A., Wilman, H.R., Dennis, A., Kelly, M., Gyngell, M.L., Neubauer, S., Bell, J.D., Banerjee, R., and Thomas, E.L. (2018). Measurement of liver iron by magnetic resonance imaging in the UK Biobank population. PLoS One *13*, e0209340.

15. Hong, C.W., Hamilton, G., Hooker, C., Park, C.C., Tran, C.A., Henderson, W.C., Hooker, J.C., Fazeli Dehkordy, S., Schwimmer, J.B., Reeder, S.B., et al. (2019). Measurement of spleen fat on MRI-proton density fat fraction arises from reconstruction of noise. Abdom Radiol (NY) *44*, 3295–3303.

16. Labranche, R., Gilbert, G., Cerny, M., Vu, K.-N., Soulières, D., Olivié, D., Billiard, J.-S., Yokoo, T., and Tang, A. (2018). Liver Iron Quantification with MR Imaging: A Primer for Radiologists. Radiographics *38*, 392–412.